

Bias in CIV-based quasar black hole mass scaling relationships from reverberation mapped samples

Michael S. Brotherton^{1*}, J. C. Runnoe^{1,2}, Zhaohui Shang³, and M. A. DiPompeo¹

¹*Department of Physics and Astronomy, University of Wyoming, Laramie, WY 82071, USA*

²*Department of Astronomy and Astrophysics, The Pennsylvania State University
525 Davey Lab, University Park, PA 16803, USA*

³*Department of Physics, Tianjin Normal University, Tianjin 300387, China*

ABSTRACT

The masses of the black holes powering quasars represent a fundamental parameter of active galaxies. Estimates of quasar black hole masses using single-epoch spectra are quite uncertain, and require quantitative improvement. We recently identified a correction for C IV $\lambda 1549$ -based scaling relationships used to estimate quasar black hole masses that relies on the continuum-subtracted peak flux ratio of the ultraviolet emission-line blend Si IV + OIV] (the $\lambda 1400$ feature) to that of C IV. This parameter correlates with the suite of associated quasar spectral properties collectively known as “Eigenvector 1” (EV1). Here we use a sample of 85 quasars with quasi-simultaneous optical-ultraviolet spectrophotometry to demonstrate how biases in the average EV1 properties can create systematic biases in C IV-based black hole mass scaling relationships. This effect results in nearly an order of magnitude moving from objects with small $\langle \text{peak } \lambda 1400 / \text{C IV} \rangle$, which have overestimated black hole masses, to objects with large $\langle \text{peak } \lambda 1400 / \text{C IV} \rangle$, which have underestimated values. We show that existing reverberation-mapped samples of quasars with ultraviolet spectra – used to calibrate C IV-based scaling relationships – have significant EV1 biases that result in predictions of black hole masses nearly 50% too high for the average quasar. We offer corrections and suggestions to account for this bias.

Key words: galaxies: active – quasars: general – accretion, accretion discs – black hole physics.

1 INTRODUCTION

Black hole mass is a fundamental quasar property, and better measuring poorly known fundamental properties has the potential to lead to breakthroughs. Moreover, correlations between the central black hole mass in galaxies, both active and inactive, and other properties such as the stellar velocity dispersion and bulge luminosity (Marconi & Hunt 2003; Tremaine et al. 2002; Kormendy & Ho 2013), may indicate a connection necessary to understanding galaxy evolution more generally.

Several methods exist to directly measure or indirectly estimate the central black hole masses of quasars (see Shen 2013 for a review). A primary method of measuring black hole masses is via reverberation mapping (RM, e.g., Peterson 1993). The underlying premise is that broad-line region (BLR) gas moves virially under gravity (Peterson & Wandel 1999, Onken et al. 2003). This means that BLR gas at a

distance R_{BLR} with a velocity ΔV can be used to provide the central mass using an equation of the form:

$$M_{\text{BH}} = f \frac{R_{\text{BLR}} \Delta V^2}{G} \quad (1)$$

The factor f includes our ignorance about geometry (and perhaps other complications), and is obtained by calibration against inactive galaxies (e.g., Onken et al. 2004).

RM programs provide the radius R_{BLR} via time lags between the continuum and line flux, while the velocity ΔV is measured from the variable portion of the emission-line profile. Both the Full Width at Half Maximum (FWHM) and the line dispersion σ_{line} of the RMS profile have been used, in conjunction with an appropriately calibrated f . We will refer to the quantity $R_{\text{BLR}} \Delta V^2 / G$ as the virial product. Numerous campaigns over more than two decades (e.g. Clavel et al. 1991; Kaspi et al. 2000, 2007; Peterson et al. 2004, Bentz et al. 2009b; Denney et al. 2010) have provided virial products for over 50 objects, which are not necessarily representative of active galaxies in general (e.g., Shen 2013).

Because of the large observational resources required for

* E-mail: mbrother@uwyo.edu

RM, easier methods of estimating black hole masses have been developed, e.g., black hole mass scaling relationships (e.g., Vestergaard 2002). Single-epoch (SE) spectra, rather than RMS spectra, provide line-profile measurements, while the radius-luminosity relationship (e.g., Kaspi et al. 2000; Bentz et al. 2006) provides R_{BLR} rather than a time lag. These two points permit the modification of equation 1 and lead to:

$$M_{\text{BH}} = f \frac{R_{\text{BLR}} \Delta V^2}{G} = f \frac{\lambda L_{\lambda}^{\gamma} \Delta V^2}{G}. \quad (2)$$

The exponent γ appears to be consistent with 0.5, at least when the host galaxy contribution to the continuum is accounted for (e.g., Bentz et al. 2009a), as expected for some simple BLR models (e.g., Netzer 1990).

In practice, the black hole mass can be calculated from the combination of the unscaled mass μ and a constant a , which provides the scaling factor:

$$\mu = \left(\frac{\Delta V}{1000 \text{ km s}^{-1}} \right)^2 \left(\frac{\lambda L_{\lambda}}{10^{44} \text{ ergs s}^{-1}} \right)^{\gamma} \quad (3)$$

$$\log M_{\text{BH}} = \log \mu + a \quad (4)$$

The scaling relationships are not very precise, unfortunately, and may not be very accurate, either, as we shall demonstrate. Black hole masses calculated with these equations are typically uncertain to factors of 3-4 (Vestergaard & Peterson 2006, hereafter VP06). Given their utility, needing only a SE spectrum, however, it is desirable to improve existing relationships (in particular for those using ultraviolet lines like C IV $\lambda 1549$, which is redshifted into the optical regime for high- z quasars). Despite possible biases in selection, RM samples have been used to calibrate the SE scaling relationships. The formulations of VP06 and Vestergaard & Osmer (2009) have been two often-employed examples. Recently Park et al. (2013), using more reliable reverberation masses and myriad small improvements, have updated the C IV-based scaling relationship.

There have been a number of concerns noted regarding black hole mass estimates using C IV (e.g., Croom 2011, Assef et al. 2011, Trakhtenbrot & Netzer 2012, etc.). The primary criticism is that the FWHM of the C IV line does not always correlate well with that of $H\beta$ in SE spectra, and that the former is often narrower than the latter, the reverse of the results for the RMS profiles from RM campaigns (e.g., Onken et al. 2004). The SE profile of C IV probably does not reflect purely virial motions. Denney (2012) compared the reverberating component of C IV against average profiles, showing evidence for a low-velocity emission-line region that did not vary, consistent with low-velocity C IV-emitting gas existing on much larger size scales (in accordance with analysis of gravitationally lensed systems, Sluse et al. 2011). These non-varying line cores can be interpreted as the “intermediate-line region” or ILR (Wills et al. 1993; Brotherton et al. 1994). Denney also showed that a profile shape parameter ($S = FWHM/\sigma_{\text{line}}$) measuring the contamination of the C IV line by this non-virial component correlates with the differences between C IV and $H\beta$ mass estimates and could perhaps be used to correct C IV-derived masses.

The degree of non-virial/ILR C IV contamination also correlates with a suite of properties collectively known as “Eigenvector 1” (hereafter EV1; see Boroson and Green

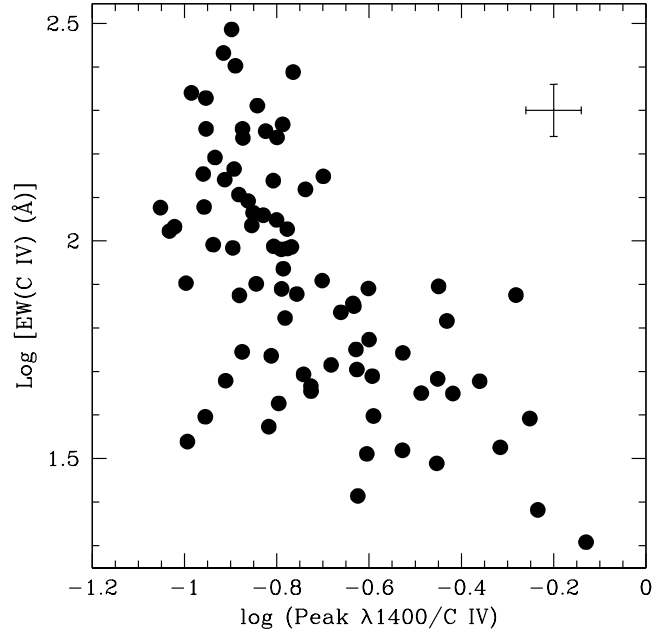


Figure 1. For the sample of Runnoe et al. (2013), we plot the log of the continuum-subtracted peak ratio of the $\lambda 1400$ feature versus the log of the rest-frame equivalent width of C IV $\lambda 1549$. This shows that the peak ratio is also associated with EV1.

1992; Brotherton & Francis 1998; Sulentic 2007; etc.). In the ultraviolet part of the spectrum, these properties include the shape of the C IV profile, as well as certain emission-line ratios and the difference between peak velocities. Shen et al. (2008; see also Shen & Liu 2012) find a bias in C IV black hole masses associated with these emission-line velocity shifts. Bian et al. (2012) also note a systematic difference between C IV and Mg II based black hole masses that related to the equivalent width of C IV, another EV1 property.

Following up on Wills et al. (1993), Runnoe et al. (2013a, hereafter Paper 1) developed a new C IV mass correction relying on the log of the ratio of the continuum-subtracted peak heights of the $\lambda 1400$ blend (of Si IV and O IV) and C IV. Figure 1 shows a significant inverse correlation between the peak ratio and the equivalent width of C IV, demonstrating that this peak ratio is also part of EV1. Paper 1 provided a mass correction term based on this peak ratio that improves the scatter between C IV and $H\beta$ derived masses by ~ 0.1 dex, or about 25%. There was also a suggestion of a bias in the VP06 C IV scaling relationship, such that C IV based masses systematically differed on average from $H\beta$, which could result in part from an EV1 bias in the RM sample that it and other scaling relationships are based upon. Figure 2, showing distributions of a primary optical EV1 parameter, peak $\lambda 5007$, for the RM sample of Park et al. (2013) and a complete sample of PG quasars Boroson & Green 1992), supports this hypothesis. Quasars from Park et al. (2013) tend to have strong [O III] $\lambda 5007$ emission, but rarely very weak [O III] $\lambda 5007$ emission, compared to the representative, complete sample.

Here we will examine quantitatively how sample biases in EV1 lead to systematic shifts in estimates of black hole

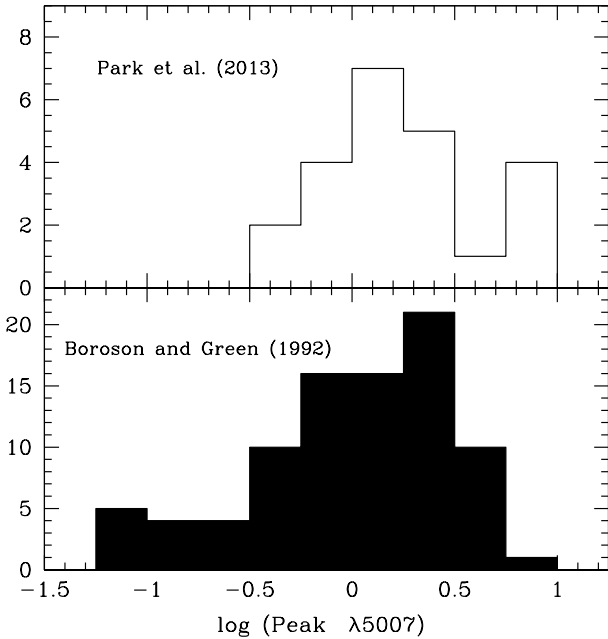


Figure 2. In the lower panel we plot the histogram of peak [O III] $\lambda 5007$, a primary optical EV1 parameter, from the complete Palomar-Green subsample of Boroson & Green (1992). The top panel shows a histogram (based on estimates from literature figures displaying spectra) for the same parameter for RM objects in the sample of Park et al. (2013), which has been used to calibrate SE C IV black hole mass scaling relationships.

mass using C IV-based scaling relationships, and the implications of this for determining what the best practices should be going forward to pursue better black hole masses. In particular we are concerned about commonly used scaling relationships based on RM samples that, while possessing superior and direct black hole mass measurements, may be biased with respect to EV1.

There may be several issues that affect SE C IV black hole mass scaling relationships, and we use a careful approach to isolate the EV1 bias. It is beneficial to use consistent calibration, measurements, and quasi-simultaneous optical-UV spectra when possible, or risk offsets associated with those issues (e.g., see Denney et al. 2009 and 2013). The presumably improved Park et al. (2013) equation results in C IV-based black hole masses systematically some 0.25 dex smaller than those of VP06, for instance.

Ideally we would use the VP06 and Park et al. (2013) data and measurements, but there are several problems with that approach. First, they did not provide the peak $\lambda 1400/\text{C IV}$ measurements we require to reproduce the Paper 1 analyses. Second, after making our own measurements as described in §2, the dispersion of peak $\lambda 1400/\text{C IV}$ in the RM objects is too small to significantly correlate with the difference between the C IV and $\text{H}\beta$ line widths as it does in our paper 1 sample. For these reasons, we will create samples matched to the RM objects with our own data in order to determine how the EV1 bias affects calculated masses. By using our own high-quality data sets and our own measurements, we can avoid inconsistency.

In §3, we determine black hole mass scaling relationships for subsamples drawn from the data set of Shang et al. (2011), each with different distributions of peak $\lambda 1400/\text{C IV}$ measurements from Paper 1, and demonstrate the effect on SE scaling relationships. We repeat the same experiment for both nearly complete samples and for a carefully selected sample sample to show the effect of an EV1 bias on existing samples of RM quasars. In §4, we discuss near-term and long-term resolutions to this problem, which will allow C IV to be used as a more effective mass estimator. Finally, §5 summarizes our conclusions.

2 DATA

2.1 SED Sample

For our analysis, we use the sample from Paper 1, that of Shang et al. (2011), which includes 85 quasars drawn from several sources. The unifying factor in assembling this composite sample was the existence of quasi-simultaneous spectrophotometry (within weeks or less), obtained in the near-ultraviolet taken with the *Hubble Space Telescope (HST)*, and in the optical from ground-based telescopes at Kitt peak National Observatory and McDonald Observatory.

One part was based on objects observed by the *Far Ultraviolet Spectroscopic Explorer, FUSE* (Moos et al. 2000), extending the spectra into the far-UV (see e.g. Shang et al. 2005). Another subsample consists of radio-loud quasars specifically selected to study orientation effects (see e.g., Wills et al. 1995, Runnoe et al. 2013b). Finally, the last subsample is 22 of 23 objects in the complete “PGX” sample (Shang et al. 2007), which may be expected to be largely unbiased with respect to quasar spectral properties.

Shang et al. (2011), Tang et al. (2012), and Paper 1 (Runnoe et al. 2013a) provide measurements and determinations of many properties of the quasars in this sample, including peak $\lambda 1400/\text{C IV}$ that is our ultraviolet EV1 indicator. A valuable property of the sample is that it includes a large range of types of quasars with diverse properties. In particular, the complete PGX sample is useful to make sure parameter space is sufficiently covered and suggestive of what the EV1 properties are of a representative quasar sample.

2.2 Reverberation-Mapped (RM) Samples

We want to know how possible biases in EV1 in heterogeneous RM samples may affect black hole masses obtained for the C IV-based scaling relationships derived from them. In order to do this, we need to know their peak $\lambda 1400/\text{C IV}$ distributions.

We use two RM samples that represent the basis for a commonly used C IV-based black hole mass scaling relationship and its recent update: VP06 and Park et al. (2013). We obtained ultraviolet spectra from the Multimission Archive at Space Telescope (MAST). These come not only from *HST* spectrographs, but also the *Hopkins Ultraviolet Telescope (HUT)*, and the *International Ultraviolet Explorer (IUE)*. In a few cases where multiple epochs of spectra were available for an object, we used the one that had the best combination

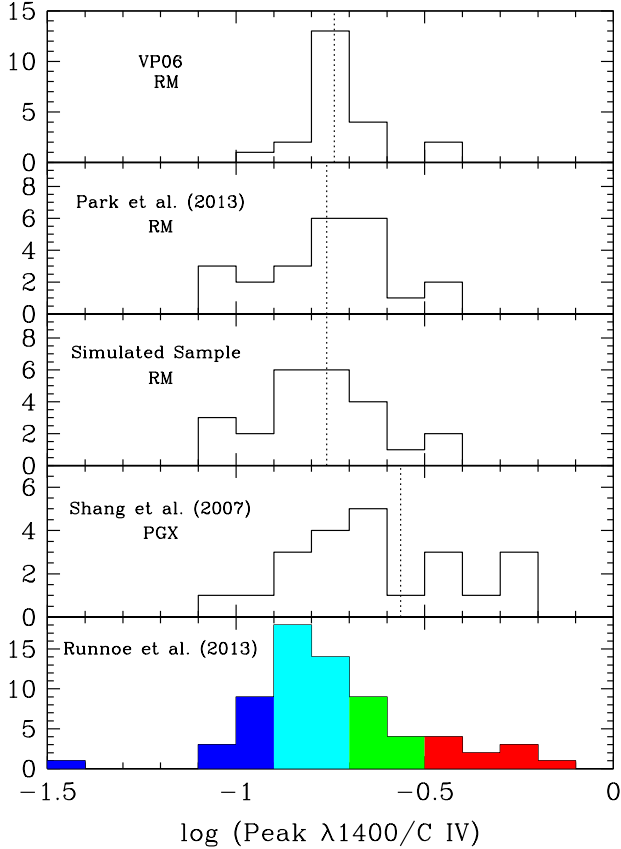


Figure 3. Histograms of peak $\lambda 1400/\text{C IV}$ for the samples used and discussed in this paper, from bottom to top: the sample of Runnoe et al. (2013), the PGX subsample of Shang et al. (2007), our subsample with peak $\lambda 1400/\text{C IV}$ matched to the Park et al. (2013) reverberation-mapped sample, and finally the reverberation-mapped samples of Park et al. (2013) and VP06. Dotted lines indicate the mean values in these panels (from top to bottom, -0.74 , -0.76 , -0.77 , and -0.56). Colors code the bottom histogram according to the $\log(\text{peak } \lambda 1400/\text{C IV})$ ratio: blue (< -0.9), cyan (from -0.9 to -0.7), green (from -0.7 to -0.5), and red (> -0.5). We will use the same colors in later figures. We draw attention to the PGX sample as being nearly complete, likely representing an unbiased distribution of peak $\lambda 1400/\text{C IV}$ and other properties.

of signal-to-noise ratio and wavelength coverage containing the $\lambda 1400$ feature.

We fit the $\lambda 1400$ feature and C IV line using a multiple Gaussian and a local continuum following the method of Tang et al. (2012) discussed in Paper 1. Fits were individually inspected to ensure that noise spikes and absorption features did not cause erroneous measurements. We checked our fitting procedure against Paper 1 for the SED sample and found agreement within the uncertainties, as well as overall systematic agreement to better than a few per cent. Our paper 1 approach was conservative, characterizing uncertainties on peak $\lambda 1400/\text{C IV}$ as $\sim 15\%$. While this ensures measurement consistency between the samples, we noted that measurements of peak $\lambda 1400/\text{C IV}$ for the same objects observed at different epochs usually agreed within

15% (e.g., Mrk 335 $- 0.16$ vs. 0.15), but not always (e.g., NGC 7469 $- 0.17$ vs. 0.10). These differences are due to real, intrinsic variability and serve as a caution to the use of non-simultaneous data. The peak $\lambda 1400/\text{C IV}$ measurements span an order of magnitude, and that the observed variability is typically much smaller than that, but this is an issue of concern to investigate in the future.

We also note that we do not include measurements for all objects in the samples of VP06 and Park et al. (2013). From VP06, we have excluded NGC 3516, NGC 4051, NGC 4151, and NGC 4593 because of absorption in C IV making a peak flux too difficult to measure reliably. Also excluded is PG 1307+085, for which the $\lambda 1400$ feature falls outside the spectral range. This leaves a sample of 22 objects in our VP06 sample. Many of the same objects are used by Park et al. (2013), however, they add PG 0804+761, Mrk 290, and NGC 4593, but exclude Mrk 110, Mrk 79, and NGC 4151. We also exclude NGC 3516, NGC 4051, and PG 1307+085 as we did from VP06 because of absorption or wavelength coverage issues that make a peak flux measurement very uncertain. Our edited Park et al. (2013) sample has 23 objects.

Table 1 lists the spectra we measured and our adopted peak $\lambda 1400/\text{C IV}$ measurements for these two samples. We do not use these peak $\lambda 1400/\text{C IV}$ measurements directly, only to select a well-matched sample with similar mean and dispersion from our SED sample for a self-consistent analysis. Table 1 includes peak $\lambda 1400/\text{C IV}$ measurements for a typical simulated RM sample matched to Park et al. (2013). Again, we want to analyze our own objects with our own consistent measurements and avoid any artificial biases associated with differences in measurement methodology.

We simulated a dozen RM samples, drawing 23 objects from the parent sample of Paper 1, matching a quasar with \log peak $\lambda 1400/\text{C IV}$ to within 0.1 dex (25%) of a corresponding object from Park et al. (2013). We selected one of these as our “simulated RM sample” on the basis of a very close match in \log peak $\lambda 1400/\text{C IV}$ (both -0.76). Our choice for illustrative RM sample also possessed the simulated sample average value of $a = 6.87$ based on intercept fitting described in § 3, and was thus representative of the simulated samples and not an outlier.

Figure 3 displays histograms of $\log(\text{peak } \lambda 1400/\text{C IV})$ for the samples of Paper 1, the PGX subsample (Shang et al. 2007), our simulated RM sample, and the VP06 and Park et al. (2013) RM samples edited as described above. Log distributions of this quantity, like some other EV1 properties such as the line ratio of $[\text{O III}]/\text{Fe II}$, appear more normally distributed than the linear values.

We also note here that the peak $\lambda 1400/\text{C IV}$ measurements from the RM samples do not correlate with the differences between the C IV and $\text{H}\beta$ line widths as they do for our sample as seen in Paper I. The lack of correlation is not inconsistent with our previous findings, but rather reflects the relatively narrow range in peak $\lambda 1400/\text{C IV}$ values. If the RM samples were unbiased, they would be expected to have mean values and distributions more closely resembling that of the PGX sample, which shows a wider range of peak $\lambda 1400/\text{C IV}$ values shifted to larger values in the histograms of Figure 3.

Table 1. Log peak $\lambda 1400/\text{C IV}$ for Reverberation-Mapped Samples

Name	peak $\lambda 1400/\text{C IV}^a$	Source (Instrument)	Date	Samples
3C 110	0.10	HST (FOS)	1995-03-16	Sim
3C 120	0.13	IUE (SWP)	1994-02-19,27; 1994-03-11	P13, VP06
3C 207	0.16	HST (FOS)	1991-12-04	Sim
3C 263	0.18	HST (FOS)	1991-11-06	Sim
3C 334	0.13	HST (FOS)	1991-09-07	Sim
3C 390.3	0.17	HST (FOS)	1996-03-31	P13, VP06
4C 01.04	0.12	HST (FOS)	1994-09-11	Sim
4C 12.40	0.16	HST (FOS)	1995-02-26	Sim
4C 41.21	0.17	HST (FOS)	1992-12-09,10	Sim
4C 49.22	0.15	HST (FOS)	1995-05-07	Sim
4C 73.18	0.16	HST (FOS)	1994-09-07	Sim
Ark 120	0.17	HST (FOS)	1995-07-29	VP06, P13
Fairall 9	0.21	HST (FOS)	1993-01-22	P13, VP06
IRAS F07546+3928	0.09	HST (STIS)	2000-01-28	Sim
Mrk 110	0.16	IUE (SWP)	1988-02-28,29	VP06
Mrk 279	0.15	HUT	1995-03-05,11	VP06
Mrk 279	0.12	HST (COS)	2011-06-27	P13
Mrk 290	0.11	HST (COS)	2009-10-28	P13
Mrk 335	0.16	HST (FOS)	1994-12-16	VP06
Mrk 335	0.15	HST (COS)	2009-10-31; 2010-02-08	P13
Mrk 509	0.18	HST (FOS)	1992-06-21	VP06
Mrk 509	0.14	HST (COS)	2009-12-10,11	P13
Mrk 590	0.21	IUE (SWP)	1991 Jan 14	P13, VP06
Mrk 79	0.17	IUE (SWP)	1979-11-15	VP06
Mrk 817	0.19	IUE (SWP)	1981-11-06,08	VP06
Mrk 817	0.24	HST (COS)	2009-08-04; 2009-12-28	P13
NGC 3783	0.16	HST (FOS)	1992-07-27	VP06
NGC 3783	0.12	HST (COS)	2011-05-26	P13
NGC 4593	0.20	HST (STIS)	2002-06-23,24	P13
NGC 5548	0.11	HST (FOS)	1993-04-26	VP06
NGC 5548	0.09	HST (COS)	2011-6-16,17	P13
NGC 7469	0.17	HST (FOS)	1996-06-18	VP06
NGC 7469	0.10	HST (COS)	2010-10-16	P13
OS 562	0.19	HST (FOS)	1992-08-11	Sim
PG 0026+129	0.16	HST (FOS)	1994-11-27	VP06, P13
PG 0052+251	0.17	HST (FOS)	1993-07-22	VP06, P13
PG 0804+761	0.31	HST (COS)	2010-06-12	P13
PG 0844+349	0.35	HST (STIS)	1999-10-21	Sim
PG 0953+414	0.17	HST (FOS)	1991-06-18	VP06, P13
PG 1100+772	0.14	HST (FOS)	1993-02-03	Sim
PG 1114+445	0.20	HST (FOS)	1996-05-13	Sim
PG 1226+023 ^b	0.35	HST (FOS)	1991-01-14,15,16	VP06, P13, Sim
PG 1229+204	0.23	IUE (SWP)	1982-05-01	VP06, P13
PG 1411+442	0.33	HST (FOS)	1992-10-03	Sim
PG 1425+267	0.14	HST (FOS)	1996-06-29	Sim
PG 1426+015	0.16	IUE (SWP)	1985-03-01,02	VP06, P13
PG 1440+356	0.30	HST (FOS)	1996-12-05	Sim
PG 1512+370	0.09	HST (FOS)	1992-01-26	Sim
PG 1613+658	0.33	IUE (SWP)	1991-02-25	VP06
PG 1613+658	0.26	HST (COS)	2010-04-08,09,10	P13
PG 1626+554	0.23	HST (FOS)	1996-11-19	Sim
PG 2130+099	0.23	HST (HRS)	1995-07-24	VP06
PG 2130+099	0.20	HST (COS)	2010-10-28	P13
PG 2214+139	0.21	HST (STIS)	2000-06-19	Sim
PG 2251+113	0.17	HST (FOS)	1991-10-23	Sim
PKS 2216-03	0.25	HST (FOS)	1992-08-27,28	Sim

^a As discussed in the text, fitting errors range up to about 15% (see also Runnoe et al. 2013), but measurements made at different epochs can differ more than this, reflecting a larger intrinsic scatter.

^b The spectrum used by VP06 and P13 does not include the $\lambda 1400$ feature, so we have used the measurement from Runnoe et al. (2013) for all samples.

3 ANALYSIS

Using our data from Paper 1, we first demonstrate quantitatively how changing the EV1 distribution systematically changes the intercept of the basic C IV black hole scaling relationships. Second, we compare the intercepts obtained for our nearly complete PGX subsample and our simulated RM subsample to determine the approximate size of the EV1 bias in black hole masses based on C IV scaling relationships from VP06 and Park et al. (2013). We conduct our analysis using both FWHM and σ_{line} .

3.1 Ultraviolet EV1 and the Intercept Bias

We first explore the effect of a bias in EV1, using different samples with systematically different peak ($\lambda 1400/\text{C IV}$), on the intercept of the C IV scaling relationship. To do this we employ the formalism of VP06 with minor modifications. We compute the unscaled mass μ from equation 3, explicitly setting the luminosity exponent $\gamma = 0.5$. Since our goal is to focus only on the effect of EV1 distributions on mass offsets, the problem is simplified if we can fix as many parameters as possible, and there is currently no evidence that the radius-luminosity relationship depends on EV1. We use both $\text{FWHM}_{C IV}$ or $\sigma_{C IV}$ in place of ΔV in separate fits.

Figure 4 plots black hole mass as determined by the $\text{H}\beta$ scaling relationship from VP06 on the Y-axis, and μ on the X-axis for both measures of ΔV using the same data and measurements as Paper 1. Symbols are coded for different ranges of peak ($\lambda 1400/\text{C IV}$) as indicated, and a typical error bar is shown for an $\text{H}\beta$ mass uncertainty of 0.4 dex (VP06) and 0.06 dex for peak ($\lambda 1400/\text{C IV}$). Strong correlations are present, consistent with Paper 1, VP06, and Park et al. (2013). Furthermore it is clear that the different subsamples are segregated, which we can quantify by determining the required intercepts to add to the unscaled mass to predict the $\text{H}\beta$ -based mass.

We used the robust least-squares fitting program GaussFit (Jefferys et al. 2013) to find a line minimizing the differences between the two sides of equation 4, allowing only the zero-point offset a to vary. We assumed typical uncertainties for all quantities, which includes M_{BH} estimates (0.43 dex, e.g. VP06) and on parameters used to compute μ (10% on ΔV and 3% on continuum luminosity – see Paper 1 and Shang et al. 2011). The fitting procedure provided the optimal offset a and a corresponding 1σ uncertainty. The fitting results are given in Table 2 and show a strong and systematic trend: as the sample mean of peak ($\lambda 1400/\text{C IV}$) increases, the intercept a decreases when using either FWHM or σ_{line} of C IV. Again using GaussFit, we computed a best-fit line to determine these relationships, for which we have assumed the standard error in the mean for the uncertainty on the log peak ($\lambda 1400/\text{C IV}$) term for each subsample, and the tabulated uncertainties on a . These fits are shown in Figure 5 and can be written for FWHM-based C IV masses:

$$a = (-1.18 \pm 0.05)(\log \text{ peak } \lambda 1400/\text{C IV}) + (6.01 \pm 0.04)(5)$$

and for σ_{line} -based C IV masses:

$$a = (-0.80 \pm 0.12)(\log \text{ peak } \lambda 1400/\text{C IV}) + (6.33 \pm 0.09)(6)$$

We note that the agreement in the slope reported in Paper 1, in the case of the FWHM-based masses, is good,

-1.18 ± 0.05 compared with -1.227 ± 0.136 (their eq. 3). In the case of σ_{line} -based C IV masses, the slope is flatter but there is less consistency, -0.80 ± 0.12 here compared to -0.220 ± 0.068 (their eq. 4). As before, we conclude this ultraviolet EV1 correction works well for FWHM-based scaling relationships, but also may be weaker when applied to σ_{line} -based scaling relationships. As discussed in Paper 1, this may be the result of FWHM being more sensitive to the EV1 variation, in the form of a non-reverberating C IV ILR component, than σ_{line} .

3.2 PGX and Reverberation-Mapped Samples

We used the above equations along with the mean values of log peak $\lambda 1400/\text{C IV}$ for the VP06 and Park et al. (2013) RM samples to estimate their zero-point offset and compare them to those of the nearly complete PGX subsample in order to compute the bias. Perhaps better, however, is to fit a directly as in equation 4 for our simulated RM sample. In any case, both approaches give similar results. See Table 3.

The mean value of log peak $\lambda 1400/\text{C IV}$ is -0.62 in the PGX sample, and -0.76 with a tighter distribution in the simulated RM sample. This latter value is consistent with the average value of -0.76 computed for the values of our edited Park et al. (2013) sample.

Taking into account that our PGX subsample is not totally complete and only 22 objects, and that we have had to edit the VP06 and Park et al. (2013) samples slightly, which are each only 23 objects, and that matching those samples can only be done approximately, we prefer to be quantitatively conservative. The zero-point offset a in the FWHM-based C IV black hole scaling relationship derived using RM samples differs from that obtained for the PGX sample, and will yield masses that are systematically high by almost ~ 0.2 dex or $\sim 50\%$. There is a similar bias for σ_{line} -based C IV masses, which is smaller but on the same order.

4 DISCUSSION

We are now entering an era of identifying first and second-order corrections to SE quasar black hole scaling relationships. Real line profiles are complex and do not seem to always represent gas moving in a purely virial manner. Moreover, accuracy and precision are both important, and efforts must be made not only to reduce scatter in scaling relationships, but also to get the zero point right. Specifically, which measurements should be made to yield the best black hole masses?

For instance, is the choice of measuring ΔV using FWHM or σ_{line} preferred? A number of articles have suggested that the latter may be a better choice (e.g. Collin et al. 2006). We have shown here σ_{line} -based masses also suffer an EV1 bias. The σ_{line} -based masses can be also biased when measured using spectra with low signal-to-noise (SNR) ratios (e.g. Denney et al 2013). Thus FWHM, being a more robust measurement for typical lower SNR quasar spectra from the Sloan Digital Sky Survey (SDSS, e.g., Shen et al. 2011) is likely preferred in that case. Working on FWHM-based scaling relationships is therefore valuable even if σ_{line} may be a less biased measurement in high-SNR spectra.

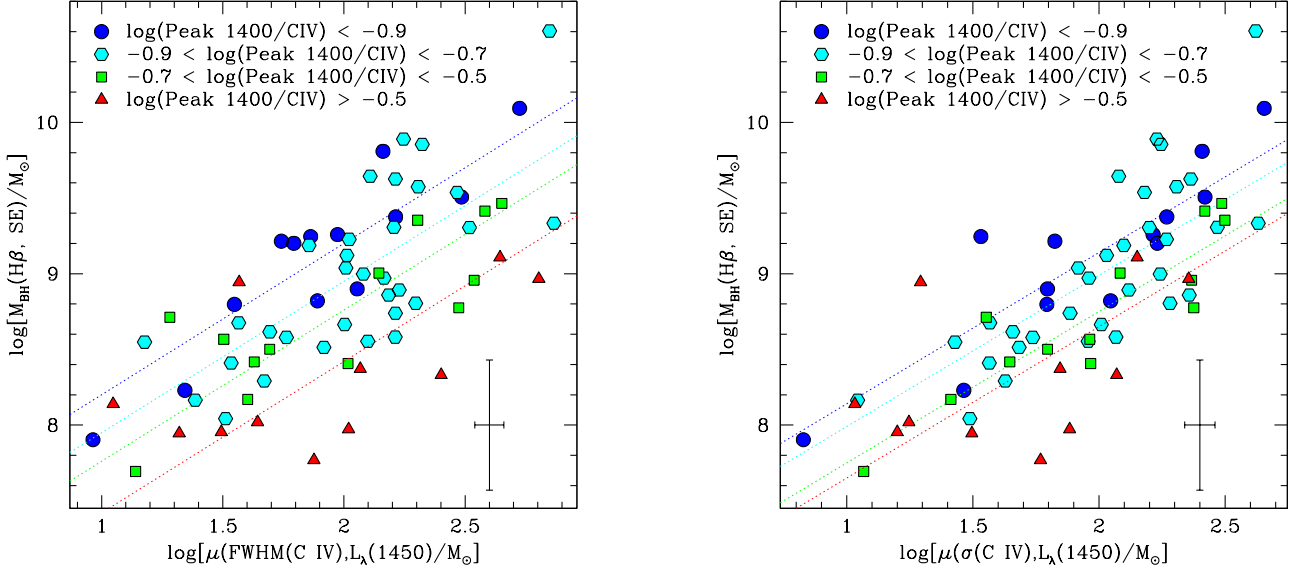


Figure 4. $H\beta$ -based single-epoch black hole masses calculated using the equation of VP06 (and tabulated by Tang et al. 2012) versus FWHM-based C IV virial products labeled μ (left panel) for the sample of Runnoe et al. (2013a). Symbols are color-coded and differently shaped according to their value of \log peak $\lambda 1400/\text{C IV}$ as in Figure 3. A conservative error bar is shown in the lower right of the figure. The right panel shows the same plot, except using a σ_{line} -based virial product.

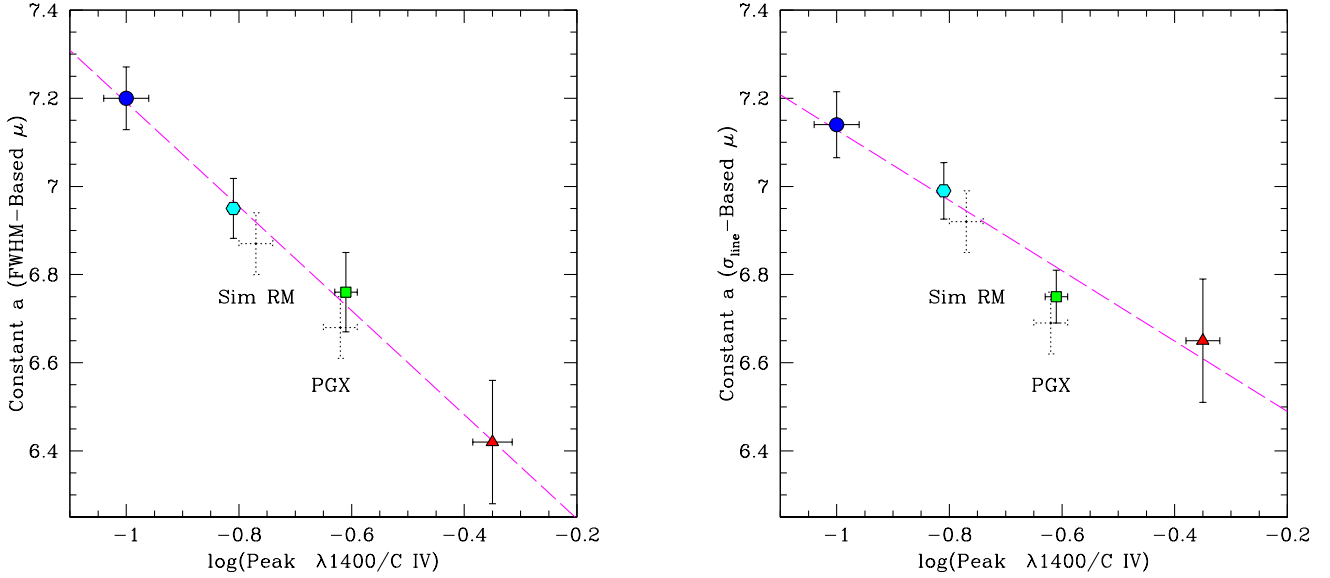


Figure 5. The fitted-line intercept a versus \log peak $\lambda 1400/\text{C IV}$ for the four binned samples, with symbols and colors to match previous figures, for the FWHM-based (left panel) and σ_{line} -based virial products. The errorbars displayed represent 1σ errors on a and the standard error of the mean for the $\log(\text{peak } \lambda 1400/\text{C IV})$ subsamples. We note the typical fitting uncertainties on a quoted by VP06 are less than 0.02 dex, much smaller than the effect illustrated here.

Table 2. C IV Mass Scaling Relationships: EV1 Subsamples and Zero Points

log peak $\lambda 1400/\text{C IV}$ Range	$\langle \log \text{Peak } \lambda 1400/\text{C IV} \rangle \pm \text{SEMean}$	N	FWHM Zero Point a	σ_{line} Zero Point a
-0.90 to -1.10	-1.00 ± 0.04	12	7.20 ± 0.07	7.14 ± 0.08
-0.70 to -0.90	-0.81 ± 0.01	32	6.95 ± 0.07	6.95 ± 0.07
-0.50 to -0.70	-0.61 ± 0.02	13	6.76 ± 0.09	6.75 ± 0.06
-0.10 to -0.50	-0.35 ± 0.04	11	6.42 ± 0.14	6.65 ± 0.14

Table 3. Zero Points for PGX and Simulated RM Samples

Sample	$\langle \log \text{peak } \lambda 1400/\text{C IV} \rangle \pm \text{SEMean}$	N	FWHM Zero Point a	σ_{line} Zero Point a
Simulated RM	-0.76 ± 0.03	23	6.87 ± 0.07	6.92 ± 0.07
PGX	-0.62 ± 0.05	22	6.68 ± 0.10	6.69 ± 0.07

4.1 Current and Future Bias Corrections

If an investigator wants the best black hole mass with only rest-frame ultraviolet spectra of low or moderate SNR, what is the best course to take?

If the object is in the SDSS Data Release 7, they can adopt the Shen et al. (2012) values already given to them, based on the VP06 prescription, but increase the value by 0.2 dex or 50% to take into account the typical EV1 bias. If they want to improve on that average EV1 correction, they can make additional measurements of the peak heights of the $\lambda 1400$ feature and C IV and apply equation 3 of Paper 1. This is also a reasonable course for updating any C IV based masses already in use that were computed using VP06 formulations.

This is probably not ideal, however, given the changes between the work of VP06 and that of Park et al. (2013), who made many small improvements that together led to significantly different C IV scaling relationships. An average correction for EV1 bias can still be applied, increasing masses by $\sim 50\%$. If measurements of the peaks of $\lambda 1400$ feature and C IV can be made, then a better, individualized correction is possible:

$$M_{\text{BH}} = M_{\text{BH}}(\text{FWHM}_{\text{C IV}}, \text{P13}) - 1.23 \log \text{peak} \frac{\lambda 1400}{\text{CIV}} - 0.91(7)$$

The above equation assumes the Paper 1 slope on the EV1 term and a RM sample mean of $\log \text{peak } \lambda 1400/\text{C IV}$ of -0.76 . While we have provided a second decimal place on the numbers in the equation, we recommend rounding results to only the first decimal place. We suggest the Paper 1 slope (-1.23 rather than -1.18) because the previous analysis does not bin data which can have a small effect on the fitted slope, and note that the larger uncertainty is the result of conservative errors on individual points compared to the actual scatter in the data points that we used for the subsamples. This equation also assumes that our EV1 correction does not change for higher luminosity, higher redshift quasars, but this should be explicitly and quantitatively investigated. The correction could change if the ‘‘Baldwin effect’’ (Baldwin 1977), the inverse correlation between emission line equivalent width and continuum luminosity, differs between C IV and the $\lambda 1400$ feature, or if it differs between the contaminating ILR component and the rest of the C IV emission line. Shang et al. (2003) found that the narrower line core of C IV correlated with luminosity in the sense of the Baldwin effect, and therefore a dependence on luminosity seems plausible, if not likely. Furthermore, at higher redshifts whatever unknown property or properties driving EV1 could differ from those in our lower redshift samples, or differ in their manifestation.

4.2 Implications for Current and Future RM Campaigns

It is not necessarily necessary to give up using RM samples to derive black hole mass scaling relationships. In principle such samples have the most reliable black hole masses and it is desirable to use them when possible. Ideally, these samples can be expanded to include a larger range in EV1, particularly objects at the narrow-line Seyfert 1 (NLS1) end of the trend at high values of $\text{peak } \lambda 1400/\text{C IV}$, that are currently underrepresented, at least in the case of also having rest-frame ultraviolet spectra covering the C IV emission line. New ultraviolet *HST* spectroscopy of NLS1s that have been reverberation mapped (e.g., Du et al. 2014) would be quite useful in expanding the sample of RM quasars with a wider range of EV1 properties. RM campaigns should, more generally, endeavour to include the full range of all types of broad-lined AGNs in order to avoid systemic biases of all types, and not just target the easiest and most cooperative objects.

We must be concerned about some NLS1s, however, given suspicions that the presence of extreme high-ionization winds emitting C IV might prevent accurate mass estimation (e.g., Vestergaard 2011). Additionally, the currently existing EV1 bias could result from a physical effect, that NLS1s may not vary as strongly as other broad-lined Seyfert Galaxies and quasars (e.g., Ai et al. 2013), making them more challenging targets for reverberation campaigns. Another potential issue is that EV1 properties may result in biases of not only the C IV derived masses, but of $H\beta$ derived masses. Du et al. (2014) find that two of their NLS1s with extremely high accretion rates have time lags significantly shorter than expected based on existing $R_{\text{BLR}} - L$ relationships, which may lead to systematic overestimation of black hole masses for similar objects using existing $H\beta$ scaling relationships. A statistically larger number of reverberation-mapped AGNs is required to more fully investigate this result.

Despite these caveats, there is reason for optimism as improvements are clear and more can be expected in the future given these and other approaches. Of particular interest is the new, large reverberation mapping effort described by Shen et al. (2015), which promises to deliver dozens of new broad-line time lags for a homogeneously selected sample of quasars likely including the full range in EV1. Quasar black hole mass determinations will improve, and RM efforts are still needed to drive improvements.

5 SUMMARY

We have explicitly demonstrated how samples biased in UV probes EV1 produce biased black hole mass scaling relationships. We have also determined quantitatively the size of the effect and its general consistent with our previous work. We have shown how to make both average and individualized

corrections to black hole masses estimated using the C IV line based on equations derived from reverberation-mapped samples, which are popular but heterogeneous and biased in EV1. They, on average, lead to mass estimates that are ~ 0.2 dex or about 50% too high.

ACKNOWLEDGMENTS

We would like to thank Kelly Denney for helpful discussions during the preparation of this work. M. S. Brotherton acknowledges support through the Space Telescope Science Institute, AURA through Grant HST-AR-13237.01-A. Z. Shang acknowledges support by the National Natural Science Foundation of China through Grant No. 10773006 and Tianjin Distinguished Professor Funds.

REFERENCES

- Ai, Y. L., Yuan, W., Zhou, H., et al. 2013, *AJ*, 145, 90
 Assef R. J., Frank S., Grier C. J., Kochanek C. S., Denney K. D., Peterson B. M., 2012, *ApJ*, 753, L2
 Bentz M. C., Peterson B. M., Netzer H., Pogge R. W., Vestergaard M., 2009a, *ApJ*, 697, 160
 Bentz M. C., et al., 2009b, *ApJ*, 705, 199
 Bian, W.-H., Fang, L.-L., Huang, K.-L., & Wang, J.-M. 2012, *MNRAS*, 427, 2881
 Boroson T. A., Green R. F., 1992, *ApJS*, 80, 109
 Brotherton M. S., Wills B. J., Francis P. J., Steidel C. C., 1994, *ApJ*, 430, 495
 Clavel J., et al., 1991, *ApJ*, 366, 64
 Collin S., Kawaguchi T., Peterson B. M., Vestergaard M., 2006, *A&A*, 456, 75
 Croom S. M., 2011, *ApJ*, 736, 161
 Denney K. D., Pogge R. W., Assef R. J., Kochanek C. S., Peterson B. M., Vestergaard M., 2013, *ApJ*, 775, 60
 Denney K. D., 2012, *ApJ*, 759, 44
 Denney K. D., Peterson B. M., Dietrich M., Vestergaard M., Bentz M. C., 2009, *ApJ*, 692, 246
 Du P., et al., 2014, *ApJ*, 782, 45
 Jefferys W., McArthur B., McCartney J., 2013, *ascl.soft*, 5009
 Kaspi S., Smith P. S., Netzer H., Maoz D., Jannuzi B. T., Giveon U., 2000, *ApJ*, 533, 631
 Kaspi S., Brandt W. N., Maoz D., Netzer H., Schneider D. P., Shemmer O., 2007, *ApJ*, 659, 997
 Kormendy J., Ho L. C., 2013, *ARA&A*, 51, 511
 Marconi A., Hunt L. K., 2003, *ApJ*, 589, L21
 Moos H. W., et al., 2000, *ApJ*, 538, L1
 Netzer, H. 1990, in *Active Galactic Nuclei, Saas-Fee Advanced Course 20*, ed. T. J.-L. Courvoisier & M. Major (Berlin: Springer), 57
 Onken C. A., Peterson B. M., Dietrich M., Robinson A., Salamanca I. M., 2003, *ApJ*, 585, 121
 Onken C. A., Ferrarese L., Merritt D., Peterson B. M., Pogge R. W., Vestergaard M., Wandel A., 2004, *ApJ*, 615, 645
 Park D., Woo J.-H., Denney K. D., Shin J., 2013, *ApJ*, 770, 87
 Peterson B. M., et al., 2004, *ApJ*, 613, 682
 Peterson B. M., Wandel A., 1999, *ApJ*, 521, L95
 Peterson B. M., Wanders I., Horne K., Collier S., Alexander T., Kaspi S., Maoz D., 1998, *PASP*, 110, 660
 Runnoe J. C., Brotherton M. S., Shang Z., DiPompeo M. A., 2013a, *MNRAS*, 434, 848
 Runnoe J. C., Brotherton M. S., Shang Z., Wills B. J., DiPompeo M. A., 2013b, *MNRAS*, 429, 135
 Shang Z., et al., 2011, *ApJS*, 196, 2
 Shang Z., Wills B. J., Robinson E. L., Wills D., Laor A., Xie B., Yuan J., 2003, *ApJ*, 586, 52
 Shang Z., Wills B. J., Wills D., Brotherton M. S., 2007, *AJ*, 134, 294
 Shen Y., et al., 2015, *ApJS*, 216, 4
 Shen Y., 2013, *BASI*, 41, 61
 Shen Y., Liu X., 2012, *ApJ*, 753, 125
 Shen Y., et al., 2011, *ApJS*, 194, 45
 Shen Y., Greene J. E., Strauss M. A., Richards G. T., Schneider D. P., 2008, *ApJ*, 680, 169
 Sluse D., et al., 2011, *A&A*, 528, A100
 Sulentic J. W., Bachev R., Marziani P., Negrete C. A., Dultzin D., 2007, *ApJ*, 666, 757
 Tang B., Shang Z., Gu Q., Brotherton M. S., Runnoe J. C., 2012, *ApJS*, 201, 38
 Trakhtenbrot B., Netzer H., 2012, *MNRAS*, 427, 3081
 Tremaine S., et al., 2002, *ApJ*, 574, 740
 Vestergaard M., 2002, *ApJ*, 571, 733
 Vestergaard M., Peterson B. M., 2006, *ApJ*, 641, 689
 Wills B. J., Brotherton M. S., Fang D., Steidel C. C., Sargent W. L. W., 1993, *ApJ*, 415, 563
 Wills, B. J., Thompson, K. L., Han, M., et al. 1995, *ApJ*, 447, 139